Table 2.11: Model for epoch 1989.26 at 10.65 GHz.

Name	S [Jy]	δ_S [Jy]	r [mas]	δ_r [mas]	θ [°]	δ_θ [°]	b_{maj} [mas]	$\delta_{b_{maj}}$ [mas]	ϵ	δ_ϵ	ϕ [°]	δ_ϕ [°]	Fit
D	1.280	0.067	0.000	0.000	0.000	0.000	0.239	0.025	0.999	0.000	110.591	0.000	G
C5	1.452	0.031	1.066	0.030	-115.128	1.555	0.672	0.030	0.210	0.045	75.455	5.288	G
C4	2.353	0.089	1.611	0.009	-101.963	0.603	0.680	0.044	0.703	0.045	-40.226	8.964	G
C3a	1.183	0.138	2.297	0.096	-101.425	1.383	1.363	0.061	0.327	0.158	102.710	8.489	G
C3	0.912	0.084	4.546	0.178	-83.750	1.780	2.621	0.391	0.736	0.140	34.671	5.103	G
C2	0.541	0.062	7.914	0.177	-74.041	1.388	2.281	0.336	0.682	0.139	0.356	7.209	G

Total flux: $S_{tot} = 7.720 \pm 0.208$

Notes: S – component flux density; r – component relative distance from the core "D"; θ – component position angle (North through West); b_{maj} – component major axis; ϵ – component axial ratio; ϕ – component major axis position angle (North through West); Fit – type of the fit (G – elliptical Gaussian; S – optically thin sphere). The δ–s indicate the estimated errors for the corresponding parameters.

September 16, 1992 (1992.71)

The map (Figure 2.17 on page 53) looks radically different from the previous epoch. The core flux dominates the emission (see Table 2.12 on page 54). C7 is already detectable at just about the smallest reliably measurable separation of 0.2 mas. At 8 GHz, C7 is much weaker ($S_8 \approx$0.5 Jy) than at 22 GHz ($S_{22} \approx$5.4 Jy in November 1992, see Table 2.8 on page 40). This is consistent with the generally accepted scheme of a relativistic shock evolution which predicts a substantial rise of high–frequency emission with subsequent shift of the spectral maximum towards lower frequencies.

Fluxes of C4 and C5 have declined since 1989, and these components have apparently already passed through their maxima at 8 GHz. C6 can be still on its rise. The twist at 5 mas distance from the core is still visible in the jet, marking the division between C5 and C4.

The RMS noise in the map is 3 mJy. With the peak flux density of 6.92 Jy it gives about 2300:1 for the dynamic range.

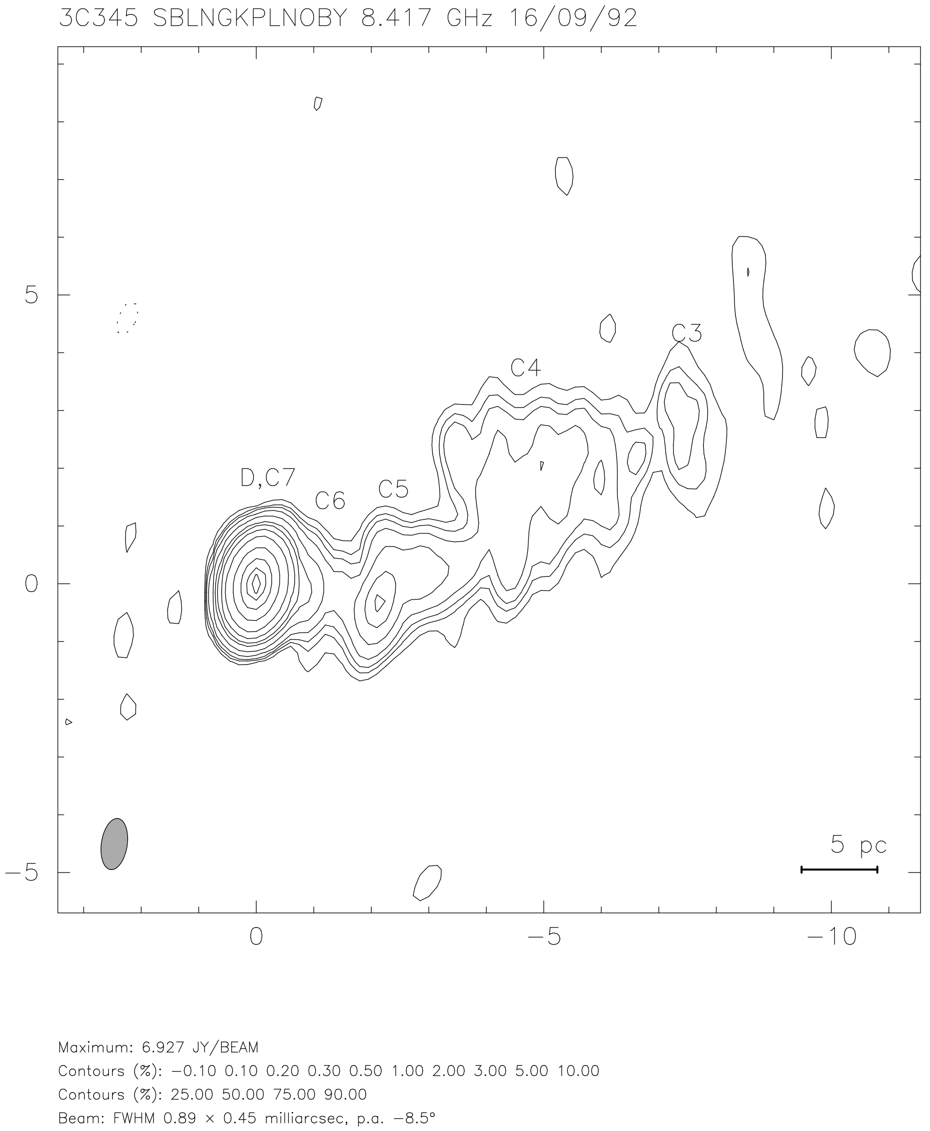

Figure 2.17: VLBI map of 3C345 observed at 8.4 GHz on September 16, 1992.

Table 2.12: Model for epoch 1992.71 at 8.41 GHz.

Name	S [Jy]	δ_S [Jy]	r [mas]	δ_r [mas]	θ [°]	δ_θ [°]	b_{maj} [mas]	$\delta_{b_{maj}}$ [mas]	ϵ	δ_ϵ	ϕ [°]	δ_ϕ [°]	Fit
D	7.831	0.200	0.000	0.000	0.000	0.000	0.307	0.019	0.664	0.050	102.657	3.564	G
C7	0.517	0.060	0.201	0.072	-102.009	12.938	0.147	0.047	0.915	0.106	171.399	0.000	G
C6	0.481	0.076	0.690	0.124	-106.488	6.576	0.259	0.081	0.949	0.186	126.637	0.000	G
C5	0.426	0.052	2.194	0.036	-97.984	1.426	0.749	0.161	0.638	0.200	-28.638	18.258	G
C4	0.902	0.081	4.389	0.237	-74.588	1.770	3.677	0.353	0.431	0.092	-56.279	8.853	G
C3	0.430	0.132	8.169	0.436	-69.512	4.533	8.020	0.850	0.365	0.185	-68.444	19.264	G

Total flux: $S_{tot} = 10.587 \pm 0.276$

Notes: S – component flux density; r – component relative distance from the core "D"; θ – component position angle (North through West); b_{maj} – component major v axis; ϵ – component axial ratio; ϕ – component major axis position angle (North through West); Fit – type of the fit (G – elliptical Gaussian; S – optically thin sphere). The δ–s indicate the estimated errors for the corresponding parameters.

November 20, 1993 (1993.88)

The map has been produced using only the VLBA antennas which resulted in decreasing the angular resolution due to the absence of intercontinental baselines. At the same time, the outstanding performance of the VLBA antennas and more adequate knowledge of variations of the antenna system temperatures during the observation have resulted in lower RMS noise and better sensitivity to extended structures in the source.

D, C7, and C6 are blended together in the map (Figure 2.17 on page 53), but their fluxes are high enough (see Table 2.12 on page 54) for model fitting to be able to detect them. The use of a smaller number of Gaussian components for modeling the blended core complex caused the closure phase fit to deteriorate. The twist in the jet is not so clearly visible as it is in the previous maps. The most likely reason for this is the lower angular resolution in this map compared to the previous maps.

In the map, the extension of the jet up to 20 mas distance from the core is detected for the first time for VLBI observations of 3C 345 at 8 GHz. C1, which is expected to be found at this distance, is very weak. Because of its weakness, model fitting fails to deduce the position and extension of C1. Our best estimates give about 20 mas for the separation, $-55°$, for the component position angle, and around 10 mas for the component size. It appears to be consistent with the detections made at 5 GHz (Unwin & Wehrle 1992) and 1.6 GHz (Matveenko *et al.* 1992).

With better sensitivity, the continuous nature of the jet becomes more evident. The jet can be pictured now not as a collection of unconnected spots, but rather as a channel pervading the surrounding media, and containing the disturbances and shocks which now appear to be in place of the former bright components or or blobs.

The RMS noise of the map is exceptionally low – $\sigma_{RMS} \approx$1.6 mJy. Given the peak flux density of 4.95 Jy, the dynamic range is about 2500:1.

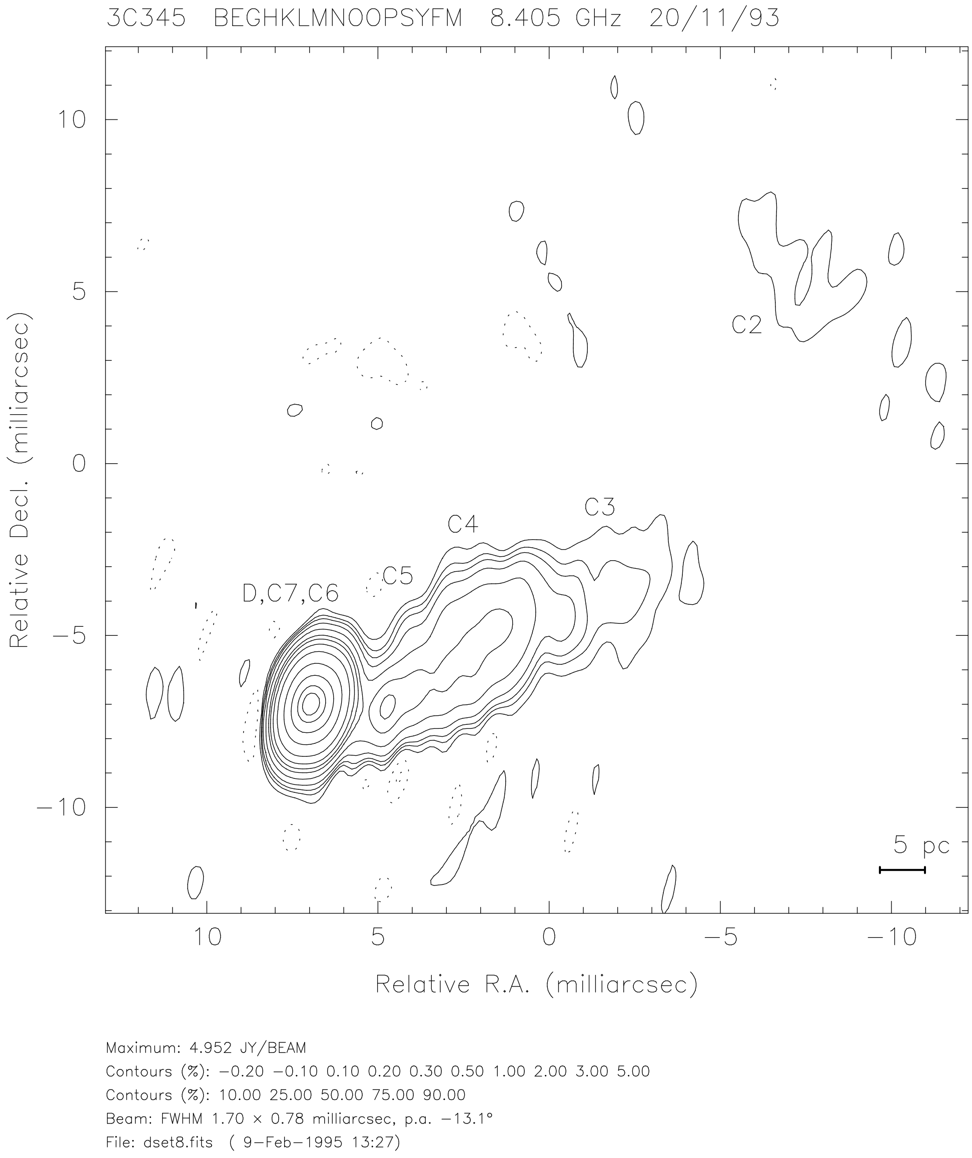

Figure 2.18: VLBI map of 3C345 observed at 8.4 GHz on November 20, 1993.

Table 2.13: Model for epoch 1993.88 at 8.40 GHz.

Name	S [Jy]	δ_S [Jy]	r [mas]	δ_r [mas]	θ [°]	δ_θ [°]	b_{maj} [mas]	$\delta_{b_{maj}}$ [mas]	ϵ	δ_ϵ	ϕ [°]	δ_ϕ [°]	Fit
D	2.576	0.115	0.000	0.000	0.000	0.000	0.000	0.000	1.000	0.000	0.000	0.000	G
C7	2.505	0.000	0.369	0.016	-93.730	3.250	0.233	0.027	0.573	0.066	117.205	9.768	G
C6	2.191	0.118	0.821	0.128	-99.170	2.841	0.207	0.034	0.893	0.442	92.241	0.000	G
C5	0.357	0.037	2.709	0.088	-89.538	1.154	1.918	0.248	0.250	0.050	109.978	5.272	G
C4	0.693	0.075	5.584	0.140	-70.881	0.724	3.106	0.213	0.613	0.042	131.461	6.732	G
C3	0.156	0.073	9.627	1.148	-72.176	2.379	4.457	0.566	0.542	0.132	108.404	15.430	G

Total flux: $S_{tot} = 8.477 \pm 0.199$

Notes: S – component flux density; r – component relative distance from the core "D"; θ – component position angle (North through West); b_{maj} – component major axis; ϵ – component axial ratio; ϕ – component major axis position angle (North through West); Fit – type of the fit (G – elliptical Gaussian; S – optically thin sphere). The δ–s indicate the estimated errors for the corresponding parameters.

Summary of the data at 8 and 11 GHz

The maps at 8 and 11 GHz confirm the conclusions about the jet morphology made from the previous observations. Better sensitivity of the latest maps at 8 GHz allow for a detection of emission at distance up to 20 mas from the core.

The jet morphology is consistent with the earlier maps made at lower frequencies. Kinks and twists of the jet are observed at the same locations at different times, and do not depend on the observing frequency. This observation suggests that the jet trajectory is steady and well–collimated.

Figure 2.19 shows the sequence maps at 8.4 and 10.6 GHz. A map at epoch 1990.84 (Unwin *et al.* 1994) is included to fill the gap in our observing epochs.

2.6.5 Observations at 5 GHz

The quality of the maps at 5 GHz is less affected by the weather conditions and insufficiency of calibration information. The dynamic ranges of the maps go as high as 9000:1, enabling reliable detections of the jet extension up to ≈25 mas distances from the core.

June 4, 1992 (1992.42)

The jet picture in the map (Figure 2.20 on page 60 is consistent with the maps mad at 8 GHz, and with the maps from Unwin and Wehrle (1992). The emission from C2 is barely at the sensitivity level of model fitting. Because of such low flux level, we cannot exclude the possibility of C2 being blended, in the model, with C3.

The C1 emission is well detected. In addition to the twist at 5 mas distance from the core, there is another twist observed at ≈15 mas from the core. At this point the jet turns approximately to the $P.A. = -40°$, the direction of the larger–scale VLBI jet observed by (Matveenko *et al.* 1992), and of the VLA jet studied by (Kollgaard *et al.* 1989). Emission from the location of C1 was also detected by Unwin and Wehrle (1992), who argued that this region might be a stationary jet feature rather than a moving component. We will return to this argument in Chapter 3.

The two features seen above and below the core complex are most likely to be artefacts arising from the calibration errors.

The Gaussian model of the source is given in Table 2.14 on page 61. Model fitting was capable of separating D, C7, and C6, despite their closeness.

The RMS noise in the map is the lowest among all the maps we have processed σ_{RMS} ≈0.4 mJy. The peak flux density is 3.17 Jy, which gives the dynamic range of 7700:1.

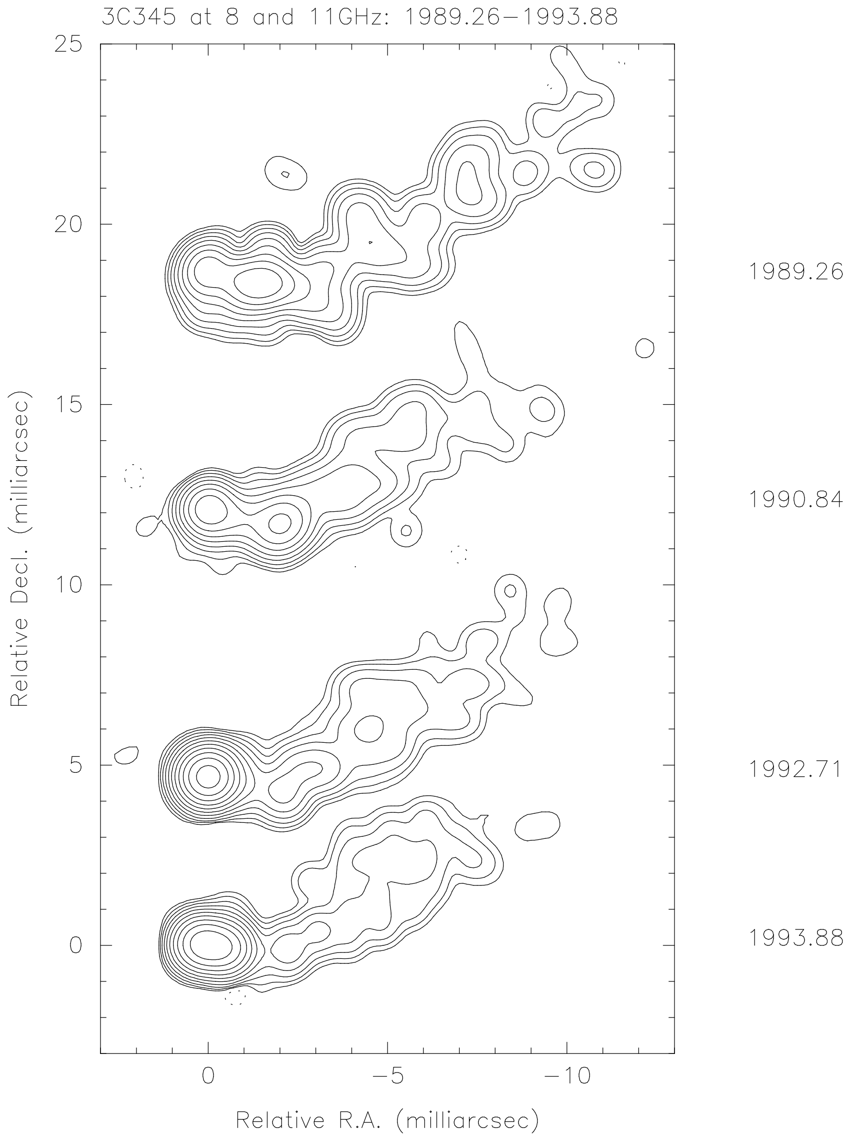

Figure 2.19: Sequence of maps at 8.4 and 10.6 GHz. Spatial separation between individual maps is proportional to the separation of the observation epochs.

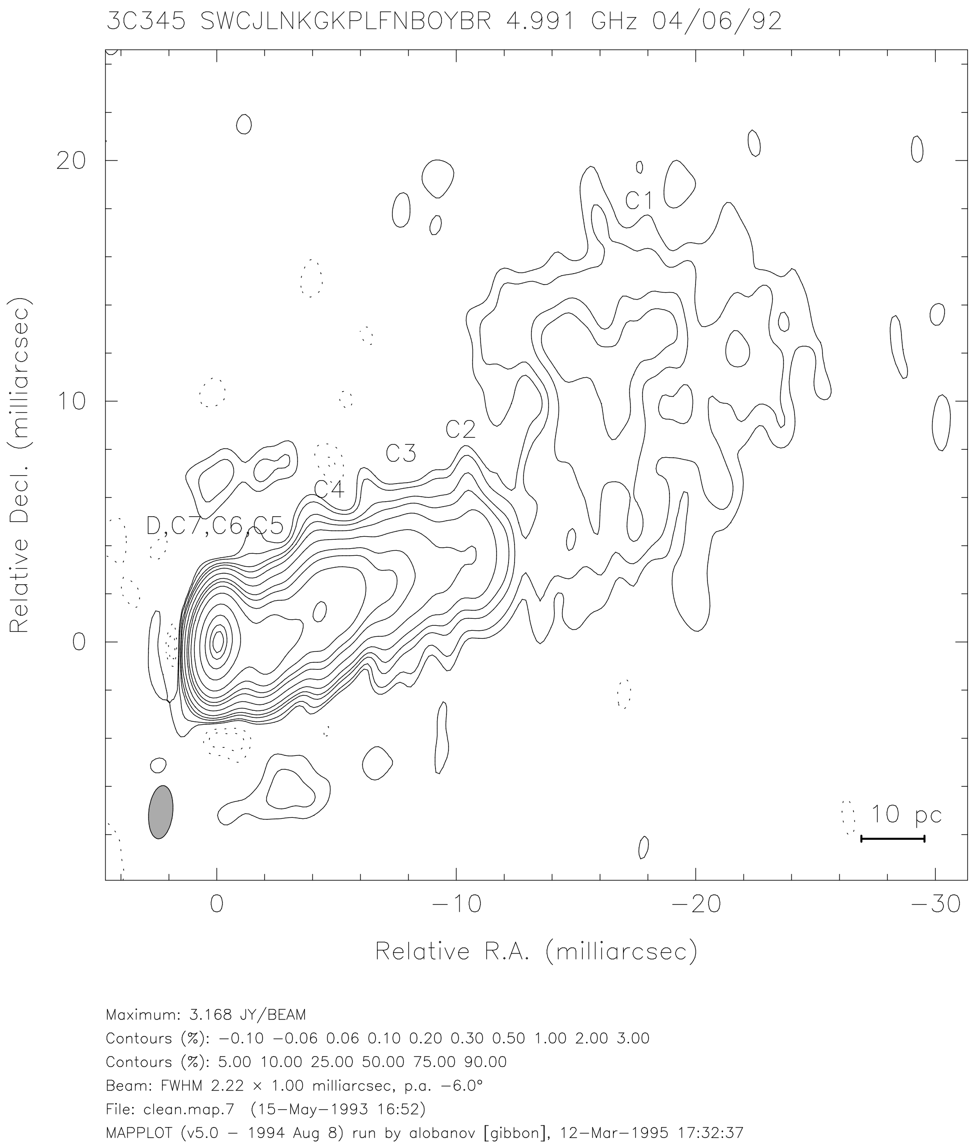

Figure 2.20: VLBI map of 3C345 observed at 5 GHz on June 4, 1992.

Table 2.14: Model for epoch 1992.42 at 4.99 GHz.

Name	S [Jy]	δ_S [Jy]	r [mas]	δ_r [mas]	θ [°]	δ_θ [°]	b_{maj} [mas]	$\delta_{b_{maj}}$ [mas]	ϵ	δ_ϵ	ϕ [°]	δ_ϕ [°]	Fit
D	2.750	0.371	0.000	0.000	0.000	0.000	0.000	0.000	1.000	0.000	28.733	0.000	G
C7	0.297	0.105	0.247	0.099	-100.920	5.603	0.149	0.039	1.000	0.000	0.000	0.000	G
C6	0.513	0.320	0.759	0.196	-94.943	5.091	0.142	0.034	1.000	0.000	89.990	0.000	G
C5	0.973	0.086	2.123	0.078	-96.863	1.225	1.434	0.144	0.100	0.000	97.145	3.449	G
C4	1.297	0.053	4.662	0.110	-72.950	1.766	3.165	0.160	0.598	0.063	117.936	5.629	G
C3	0.300	0.050	7.539	0.471	-70.633	3.223	3.628	0.390	0.596	0.062	92.337	9.978	G
C2	0.141	0.046	10.635	0.474	-69.289	6.863	3.322	0.494	0.748	0.097	62.573	7.094	G
C1	0.326	0.092	20.007	1.294	-57.829	3.632	10.025	0.841	0.796	0.296	-18.271	6.1872	G

Total flux: $S_{tot} = 6.595 \pm 0.517$

Notes: S – component flux density; r – component relative distance from the core "D"; θ – component position angle (North through West); b_{maj} – component major axis; ϵ – component axial ratio; ϕ – component major axis position angle (North through West); Fit – type of the fit (G – elliptical Gaussian; S – optically thin sphere). The δ–s indicate the estimated errors for the corresponding parameters.

June 16, 1993 (1993.45)

The map (Figure 2.21 on page 63) shows a smooth jet which turns twice — at 5 mas separation from the core, and at 15 mas separation from the core. The picture is very consistent with the one from June 1992. The model fit (see Table 2.15 on page 64) fails to detect motions in C6 and C7 with respect to their positions in June 92. Motions of the C5, C4, however, are detected and exceed the map resolution of 0.14 mas. Position changes in C3 are within the model errors. C1 appears to have its position unchanged.

The RMS noise level is 0.6 mJy. The peak flux density is 5.337 Jy, which results in the dynamic range of 8900:1 — the highest among the observations presented in the dissertation.

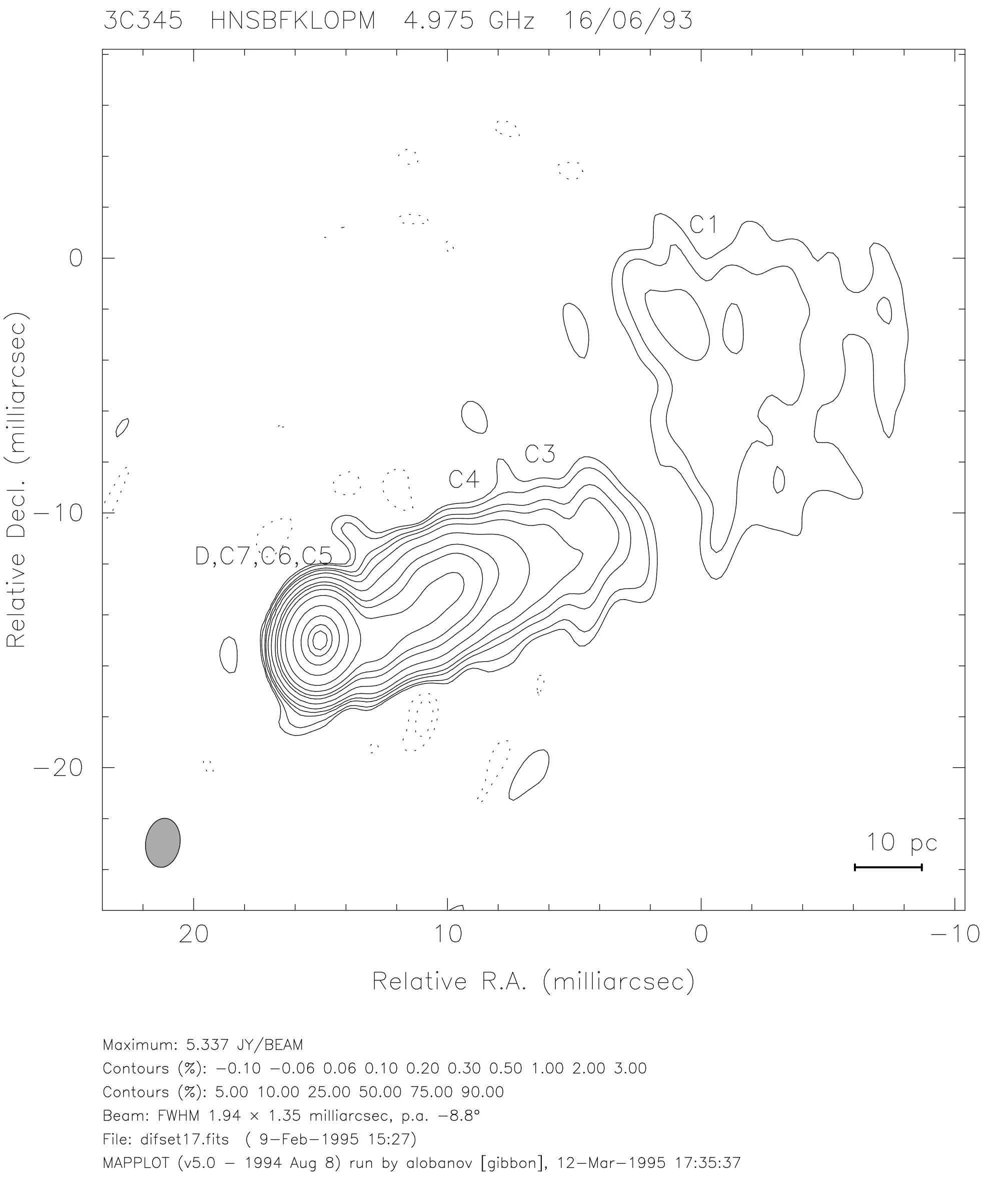

Figure 2.21: VLBI map of 3C345 observed at 5 GHz on June 16, 1993.

Table 2.15: Model for epoch 1993.45 at 4.97 GHz.

Name	S [Jy]	δ_S [Jy]	r [mas]	δ_r [mas]	θ [°]	δ_θ [°]	b_{maj} [mas]	$\delta_{b_{maj}}$ [mas]	ϵ	δ_ϵ	ϕ [°]	δ_ϕ [°]	Fit
D	1.480	0.184	0.000	0.000	0.000	0.000	0.000	0.000	1.000	0.000	0.000	0.000	G
C7	2.257	0.077	0.280	0.068	-108.848	6.196	0.171	0.000	0.900	0.000	40.613	0.000	G
C6	1.963	0.080	0.671	0.075	-96.166	7.951	0.241	0.064	0.763	0.083	117.303	6.829	G
C5	0.709	0.080	2.311	0.140	-92.396	1.962	2.265	0.293	0.163	0.034	101.631	3.313	G
C4	0.974	0.058	5.299	0.124	-71.335	0.757	3.052	0.108	0.632	0.051	123.740	4.543	G
C3	0.358	0.076	8.419	0.687	-70.839	1.393	6.375	0.895	0.373	0.079	105.515	6.442	G
C1	0.252	0.037	19.821	0.688	-56.889	2.318	8.927	0.836	0.889	0.102	21.623	6.347	G

Total flux: $S_{tot} = 7.994 \pm 0.251$

Notes: S – component flux density; r – component relative distance from the core "D"; θ – component position angle (North through West); b_{maj} – component major axis; ϵ – component axial ratio; ϕ – component major axis position angle (North through West); Fit – type of the fit (G – elliptical Gaussian; S – optically thin sphere). The δ–s indicate the estimated errors for the corresponding parameters.

September 11, 1993 (1993.69)

The map in Figure 2.22 (page 66) looks noisier than the previous one. The source has become weaker; and despite the low RMS noise level of 0.6 mJy, the side lobes are more prominent. C1 is not seen as clearly as before, partly because of the lower dynamic range of the map, and partly due to the fact that its brightness has decreased (see Table 2.16 on page 67).

The motions of C7, and C6 are still undetectable with respect to the two other maps at 5 GHz. Changes of positions in C3, and C1 are well within the model errors.

The peak flux density of the source is 3.63 Jy, which results in the dynamic range of about 6000:1.

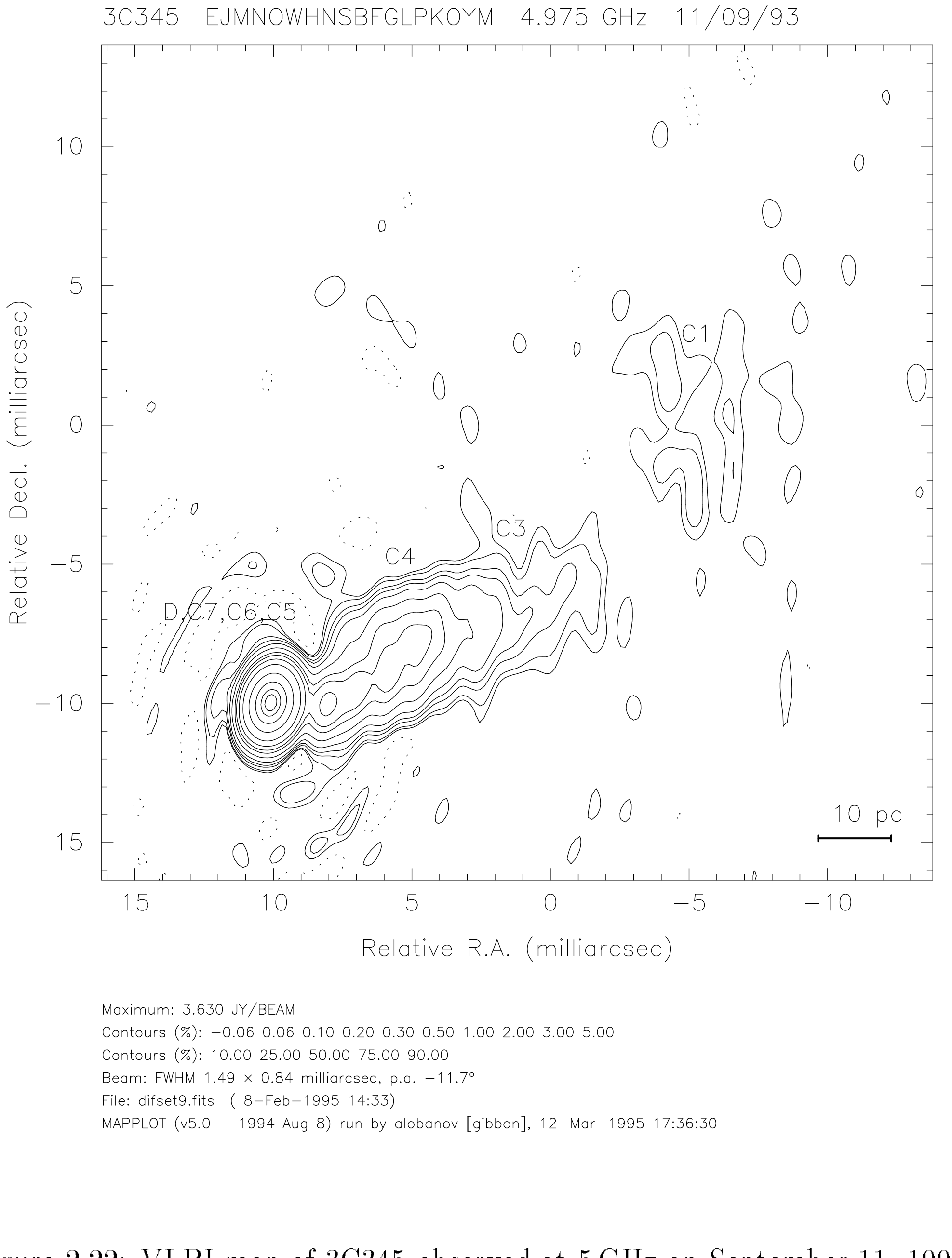

Figure 2.22: VLBI map of 3C345 observed at 5 GHz on September 11, 1993.

Table 2.16: Model for epoch 1993.69 at 4.97 GHz.

Name	S [Jy]	δ_S [Jy]	r [mas]	δ_r [mas]	θ [°]	δ_θ [°]	b_{maj} [mas]	$\delta_{b_{maj}}$ [mas]	ϵ	δ_ϵ	ϕ [°]	δ_ϕ [°]	Fit
D	1.263	0.061	0.000	0.000	0.000	0.000	0.000	0.000	1.000	0.000	0.000	0.000	G
C7	1.634	0.011	0.292	0.083	-93.358	7.012	0.153	0.076	1.000	0.000	0.000	0.000	G
C6	1.791	0.452	0.758	0.102	-97.980	4.562	0.168	0.054	1.000	0.000	0.000	0.000	G
C5	0.521	0.024	2.442	0.069	-91.570	1.009	2.218	0.117	0.223	0.041	105.922	2.706	G
C4	0.735	0.024	5.396	0.115	-70.858	0.963	3.138	0.222	0.623	0.044	129.636	7.427	G
C3	0.277	0.031	8.521	1.932	-71.048	2.367	6.268	0.379	0.360	0.097	105.142	8.854	G
C1	0.196	0.038	19.973	0.869	-56.657	3.583	10.370	0.835	0.686	0.212	18.742	0.000	G

Total flux: $S_{tot} = 6.416 \pm 0.460$

Notes: S – component flux density; r – component relative distance from the core "D"; θ – component position angle (North through West); b_{maj} – component major axis; ϵ – component axial ratio; ϕ – component major axis position angle (North through West); Fit – type of the fit (G – elliptical Gaussian; S – optically thin sphere). The δ–s indicate the estimated errors for the corresponding parameters.

Summary of the data at 5 GHz

The maps at 5 GHz show clearly the continuity of the jet at angular scales of up to 25 mas which translates into linear extension of at least 120 pc (calculated without taking into account the jet three–dimensional orientation). Along its full extension, the jet turns twice at distances of 5 and 15 mas from the core. The turns are observed at all three epochs and do not seem to be associated with any specific feature of the jet. The latter can suggest that the jet is likely to propagated within a steady environment such that the confinement of the jet does not change with time significantly.

Figure 2.23 shows the sequenc of maps at 5 GHz.

2.7 Summary

In this chapter, we have presented the maps of 3C345 from VLBI observations made during the last six years. The information obtained from the maps can be used for measuring proper motions, size and flux evolutions of the bright features embedded in the parsec–scale jet of 3C345. In order to study long–term evolution of the jet, we will combine these new observations with the existent data from the previous works. We will use the results of model fitting made by Biretta, Moore, and Cohen (1986), Krichbaum *et al.* (1991), Unwin and Wehrle (1992), Zensus, Cohen, and Unwin (1995). The models adopted from the abovementioned works are listed in Appendix A.

The overall good quality and high dynamic ranges of the maps also provide us with an opportunity of using them for quantitative multi frequency analyses which will include spectral index mapping and calculations of the jet synchrotron spectrum parameters.

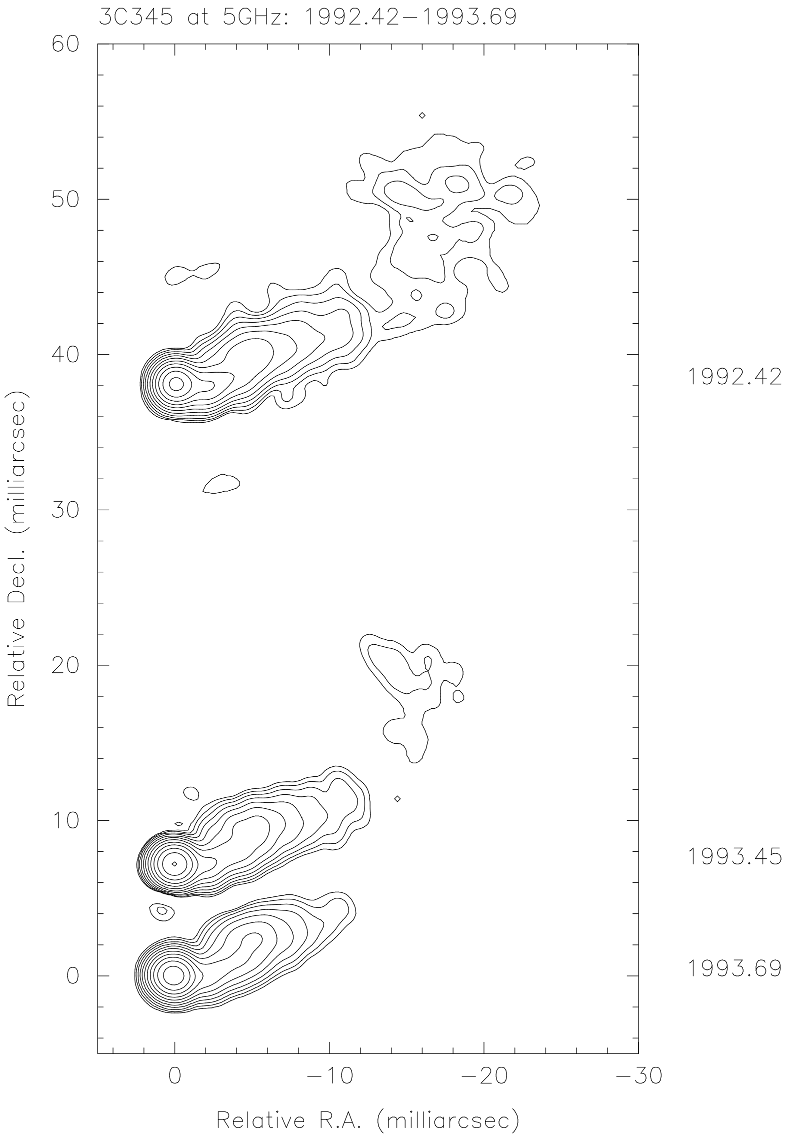

Figure 2.23: Sequence of maps at 5 GHz. Spatial separation between individual maps is proportional to the separation of the observation epochs.